2-2012

3-D Mesoscale MHD Simulations of Magnetospheric Cusp-Like Configurations: Cusp Diamagnetic Cavities and Boundary Structure

E. Adamson
University of Alaska, Fairbanks

A. Otto
University of Alaska, Fairbanks

K. Nykyri
Embry-Riddle Aeronautical University, nykyrik@erau.edu

Ann. Geophys., 30, 325–341, 2012
www.ann-geophys.net/30/325/2012/
doi:10.5194/angeo-30-325-2012

Annales Geophysicae

3-D mesoscale MHD simulations of magnetospheric cusp-like configurations: cusp diamagnetic cavities and boundary structure

E. Adamson[1,*], **A. Otto**[1], **and K. Nykyri**[2]

[1]Geophysical Institute, University of Alaska Fairbanks, Fairbanks, AK, USA
[2]Embry-Riddle Aeronautical University, Daytona-Beach, FL, USA
[*]now at: Max-Planck-Institut für Sonnensystemforschung, Katlenburg-Lindau, Germany

Correspondence to: E. Adamson (adamson@mps.mpg.de)

Received: 2 September 2011 – Revised: 23 December 2011 – Accepted: 23 January 2012 – Published: 8 February 2012

Abstract. We present results from mesoscale simulations of the magnetospheric cusp region for both strongly northward and strongly southward interplanetary magnetic field (IMF). Simulation results indicate an extended region of depressed magnetic field and strongly enhanced plasma β which exhibits a strong dependence on IMF orientation. These structures correspond to the Cusp Diamagnetic Cavities (CDC's). The typical features of these CDC's are generally well reproduced by the simulation. The inner boundaries between the CDC and the magnetosphere are gradual transitions which form a clear funnel shape, regardless of IMF orientation. The outer CDC/magnetosheath boundary exhibits a clear indentation in both the x-z and y-z planes for southward IMF, while it is only indented in the x-z plane for northward, with a convex geometry in the y-z plane. The outer boundary represents an Alfvénic transition, mostly consistent with a slow-shock, indicating that reconnection plays an important role in structuring the high-altitude cusp region.

Keywords. Magnetospheric physics (Magnetopause, cusp, and boundary layers; Solar wind-magnetosphere interactions) – Space plasma physics (Magnetic reconnection)

1 Introduction

The interaction between the solar wind and the Earth's magnetosphere is characterized by processes which occur at the magnetopause boundary. The magnetospheric cusps play a pivotal role in understanding these processes, as the entire magnetopause maps through these key regions. Extensive research has focused on the low and mid altitude cusp (Newell et al., 1989; Lockwood and Smith, 1992; Yamauchi et al., 1996), but more recently research efforts have increased focus on the high-altitude cusp region. It is important to note that differing definitions of the high altitude cusp regions have lead to confusion in the past. For example, Trattner et al. (2006) identify the high altitude cusp by the presence of inflowing plasma resulting from reconnection as indicated by the time-of-flight effect or velocity filter effect (Rosenbauer et al., 1975; Onsager et al., 1993), while Peterson and Trattner (2011) identify the region by the presence of a mixture of boundary layer and newly reconnected solar wind plasma similar to the criteria used by Newell et al. (2004). We focus our identification of the exterior cusp on the typical low magnetic field region or Cusp Diamagnetic Cavity (CDC) similar to Chen et al. (1998); Fritz et al. (2003); Niehof et al. (2008); Lavraud et al. (2002); Nykyri et al. (2011a). These CDC's are characterized by magnetosheath-like plasma density, enhanced thermal pressure and low, fluctuating magnetic field. As a result of the relatively low magnetic field magnitude within these CDC's, they are highly dynamic regions. Both the location and structure of the high-altitude cusp are known to exhibit a strong dependence on the Interplanetary Magnetic Field (IMF) (Newell et al., 1989; Woch and Lundin, 1992; Newell and Meng, 1994; Yamauchi and Lundin, 1994; Yamauchi et al., 1996; Savin et al., 1998; Fedorov et al., 2000; Dubinin et al., 2002).

The exterior cusp has been shown to have three boundaries (Lavraud et al., 2004a; Paschmann et al., 1976; Haerendel et al., 1978; Onsager et al., 2001): the day-side plasma sheet on the sunward side, the tail-lobe or mantle on the night-side, and the magnetosheath in the exterior. Though it has been suggested that the outer boundary may represent an intermediate or slow transition (Lavraud et al., 2002)

the exact nature of these boundaries is not well understood (Walters, 1966; Scarf et al., 1974; Hansen et al., 1976; Yamauchi and Lundin, 1997; Savin et al., 1998). It appears that the inner boundaries of the high-altitude cusp form a funnel shape and thus represent an indented surface which has been labelled as the magnetopause by some (Paschmann et al., 1976; Haerendel et al., 1978; Russell, 2000). However, it is not clear whether the same is true of the outer boundary between the cusp and magnetosheath. This question regarding the shape of the magnetopause in the vicinity of the cusp has persisted for some time. While some results show clear evidence of an indented surface (Zhang et al., 2007; Dunlop et al., 2005; Eastman et al., 2000), others do not (Zhou and Russell, 1997; Lavraud et al., 2004a). This debate is further complicated by the ambiguity of the definition of the magnetopause in the vicinity of the cusp, which may explain some of the disagreement.

In this paper, results are presented from a mesoscale cusp-like magnetic field model (Adamson et al., 2011). The Earth's dipole tilt is neglected in the model. This simplification of the system is partially a consequence of the desired size of the simulation domain which enables a high resolution in comparison to global models, but also matter of convenience. We note that this simplification provides a convenient foundation for future work addressing the effects of variations to the model such as the inclusion of the dipole tilt. As a result of the neglect of the dipole tilt the system has a tendency to localize the reconnection site somewhat closer to the cusp than is the case in the physical magnetosphere. Though the exact location of the reconnection site is not accurately represented in regards to the overall global structure of the Earth's magnetosphere, it is not the goal of this study to address plasma transport between the cusp and the magnetosphere on such a global scale, but rather to investigate the magnetospheric structures local to the cusp region. The physical processes responsible for the formation of the various boundary structures under investigation herein are the result of the local interaction of the shocked solar wind with the cusp region magnetosphere. Thus, it is expected that results do not exhibit any significant dependence on the geomagnetic dipole tilt other than possibly in regards to the geometry of the high latitude magnetopause.

Thus, particularly for southward IMF, the reconnection site is localized to high latitudes. Results focus on the high altitude cusp region for both strongly northward and strongly southward IMF orientations. A detailed comparison of the resulting cusp regions is presented. The boundaries of the CDC are discussed in detail and variance analysis methods (Sonnerup and Cahill, 1967) applied in order to address the nature of the boundaries. We utilize these methods to determine the boundary normals based on both the minimum variance of the magnetic field (MVAB) and on the maximum variance of the electric field (MVAE). We note that it is possible, due to the coplanarity of the magnetic field across a shock, that MVAB may determine the wrong normal eigenvector. For this reason, we give preference to the normal eigenvector resulting from MVAE.

The model and numerical method are reviewed in Sect. 2. Section 3 focuses on simulation results, separated by northward and southward IMF, followed by discussion in Sect. 4.

2 Numerical procedure

2.1 Numerical method

The presented simulation results employ the full set of MHD equations in the following form:

$$\begin{aligned} \frac{\partial \rho}{\partial t} &= -\nabla\cdot(\rho \boldsymbol{u}), \\ \frac{\partial(\rho \boldsymbol{u})}{\partial t} &= -\nabla\cdot\left[\rho \boldsymbol{u}\boldsymbol{u} + \frac{1}{2}\left(p+\boldsymbol{B}^2\right)\boldsymbol{I} - \boldsymbol{B}\boldsymbol{B}\right], \end{aligned} \tag{1}$$

$$\begin{aligned} \frac{\partial h}{\partial t} &= -\nabla\cdot(h\boldsymbol{u}) - \frac{\gamma-1}{\gamma}h^{1-\gamma}\eta \boldsymbol{j}^2, \\ \frac{\partial \boldsymbol{B}}{\partial t} &= -\nabla\times(\boldsymbol{u}\times\boldsymbol{B} - \eta \boldsymbol{j}), \\ \boldsymbol{j} &= \nabla\times\boldsymbol{B}, \end{aligned} \tag{2}$$

where $h=(p/2)^{1/\gamma}$ and ρ, p, η, $\boldsymbol{u}$, and $\boldsymbol{B}$ represent density, pressure, resistivity, velocity, and magnetic field. The ratio of specific heats (γ) is taken to be $5/3$. The resistivity (η) is held constant and is defined according to:

$$\eta = \eta_o\left[\eta_1 + \frac{1}{2\cosh((z_{\min}-z)/2)} + \frac{1-\tanh(z+.5)}{2\cosh\left((x^2+y^2)/2\right)}\right], \tag{3}$$

where $\eta_o = 0.015$ and $\eta_1 = 0.13$ in normalized simulation units. The first term defines a uniform background resistivity, while the second term prescribes a resistivity which falls off with increasing z, and the third term generates a column of resistivity aligned with the converging dipolar field in the center of the lower half of the simulation domain. As defined by this distribution, the resistivity ranges from a maximum value of 0.0245 at the center of the lower z-plane, to a minimum of 0.002 throughout the upper portion of the simulation domain towards the maximum z-boundary. This resistivity distribution improves code stability in the region of converging dipolar field while maintaining a relatively low resistivity ($\sim$0.002) near the x-line. All variables are normalized to typical system values, and thus dimensionless. Length scale, density, and magnetic field strength are normalized to typical system values ($L_0 = 1\,R_{\rm E}$, $\rho_0 = 2.0\,{\rm cm}^{-3}$, and $B_0 = 40\,{\rm nT}$). The pressure, velocity and time scale are then measured in units of normalized pressure $p_0 = B_0^2/8\pi = 0.64\,{\rm nPa}$, Alfvén speed $u_{\rm A} = B_0/\sqrt{4\pi\rho_0} = 616\,{\rm km\,s}^{-1}$, and Alfvén time $\tau_{\rm A} = L_0/u_{\rm A} = 10\,{\rm s}$, respectively.

The simulations use a Leapfrog/DuFort-Frankel finite difference scheme which is second order accurate, easy to implement, and has low numerical dissipation (the leading term in the truncation error of the DuFort-Frankel scheme varies

as Δx^2, Δt^2, but is also dependent on the diffusion coefficient η, ensuring that the physical resistivity η remains orders of magnitude larger than the numerical diffusion). The nonuniform grid has the best resolution in x and y-directions ($\Delta x,\ \Delta y = 0.08\ R_E$) in the center of the simulation domain, and the lowest ($\Delta x,\ \Delta y = 0.381\ R_E$) at the edges. The resolution in the z-direction is more uniform, with a maximum resolution of $\Delta z = 0.05\ R_E$ in the center and minimum resolution of $\Delta z = 0.163\ R_E$ at the boundaries. The grid is chosen to be more uniform in the z-direction in order to resolve not only the strong gradients toward the bottom of the domain where the field lines converge, but also the gradients within the magnetopause current sheet. The simulations presented herein are comprised of $153 \times 153 \times 153$ grid points in x, y, and z, respectively. Higher resolution ($253 \times 253 \times 203$ grid points) simulations were also undertaken in order to investigate the effect of larger density anisotropy between the magnetosphere and magnetosheath, the results of which are addressed in the next section.

The local model of the magnetospheric cusp region is constructed by placing a dipole at $-10\ R_E$ along the z-axis with the dipole axis anti-parallel to z (no dipole tilt). The coordinates are such that the x-axis is directed toward the sun and the y-axis completes the right-handed system. The simulation domain ranges from $-12\ R_E$ to $12\ R_E$ in both the x- and y-directions and the z-coordinate from $-6\ R_E$ to $6\ R_E$, such that the dipole is $4\ R_E$ below the lower z-boundary. The dipolar magnetic field is effectively turned off in the upper region of the simulation domain ($z > 0$), thus defining the magnetosheath region. This is accomplished through the inclusion of a shielding current. A constant "draped" (no z-component) IMF may then be superposed in the magnetosheath region. The x-component of this "fully-draped" model IMF then represents the combined x- and z-components of the physical IMF. Finally, the density and pressure are prescribed as functions of the magnetic field-line equation. A ballistic relaxation is then applied in order to produce a near-equilibrium configuration. For further details on the model and relaxation method see Adamson et al. (2011).

Neumann boundary conditions are imposed, such that $\partial f / \partial x_n = 0$. The normal components of the magnetic field at the boundaries are calculated such that $\nabla \cdot \boldsymbol{B} = 0$ (excluding the lower z-boundary where $\boldsymbol{B}$ is held fixed), while a simple extrapolation method is applied to the transverse components.

3 Results

Simulation results are presented, herein, for the cases of strongly northward and strongly southward IMF. Simulations are initialized with a uniform magnetosheath flow of local Alfvén Mach number (M_A) between .4 and 1 (specific values corresponding to the individual runs are indicated in the proceeding sections). The flow is prescribed as a slab corresponding to the region of draped IMF (magnetosheath).

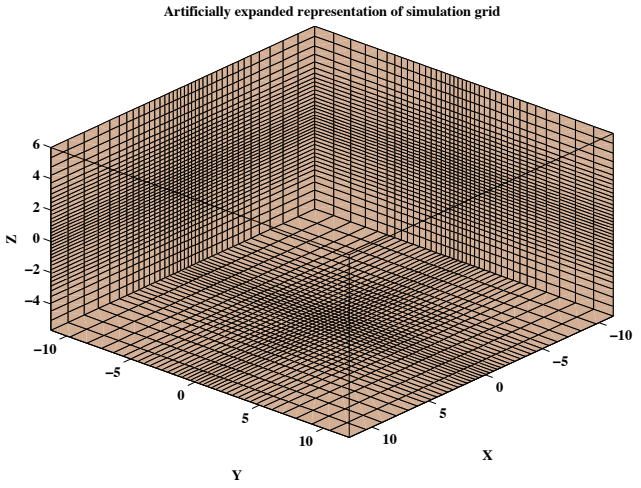

Fig. 1. Illustration of the numerical grid. Note that only every fourth grid point is plotted in order to improve visual clarity.

We define the cusp to be the "funnel"-shaped region of the magnetosphere aligned with the magnetic dipole axis and exhibiting enhanced plasma density and thermal pressure. The CDC's then, as features embedded within the cusp region must similarly satisfy the same criteria. In addition to these requirements, the CDC's typically exhibit further increased (relative to the cusp proper) and varying densities as well as significantly reduced magnetic field strength. Typical features of CDC's as identified from spacecraft observations may be summarized as follows:

1. Densities comparable to magnetosheath values (typically a factor of ten greater than adjacent magnetospheric values)
2. Significantly depressed magnetic field
3. Pervasive magnetic field fluctuations
4. Relatively stagnant plasma (for northward IMF)
5. Gradual inner boundaries with magnetosphere exhibiting clear field-aligned plasma flows emanating from reconnection site
6. Often more abrupt outer boundary with magnetosheath

3.1 CDC dependence on IMF orientation

The orientation of the IMF is widely known to exert control over the location and dynamics of the polar cusp (Carbary and Meng, 1986; Escoubet and Bosqued, 1989; Woch and Lundin, 1992; Newell and Meng, 1994; Sandholt et al., 1994; Zhou et al., 2000; Bosqued et al., 2005; Pitout et al., 2006a,b; Escoubet et al., 2008). This effect of IMF orientation on cusp

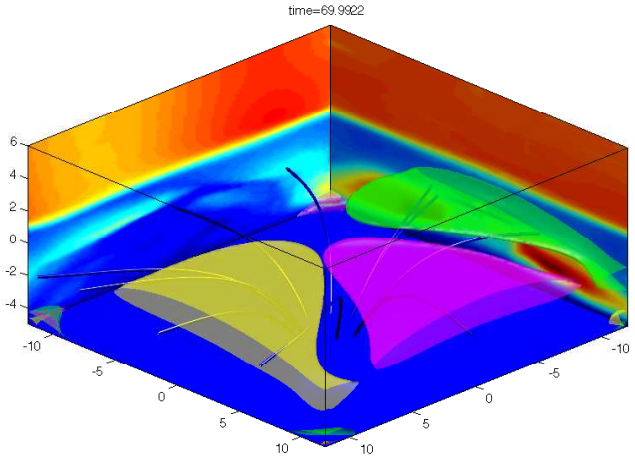

Fig. 2. Distribution of diamagnetic cavity position as indicated by high β region of cusp for strongly northward (green), purely $+B_{y_{IMF}}$ (magenta), and strongly southward IMF (yellow).

location is clearly seen in the simulation results plotted in Fig. 2. The figure shows isosurfaces encompassing the region of plasma $\beta > 30$ for three IMF orientations: 10° northward (green), 90° purely $+B(\mathrm{IMF})_y$ (magenta), and 170° southward (yellow). Plasma β is defined as the ratio of plasma thermal to magnetic pressure ($2\mu_0 P/B^2$) and is thus a useful parameter to employ in the identification of cusp diamagnetic cavities due to the characteristic enhanced plasma pressure and strongly depressed magnetic field strength within. These results indicate that the location of the CDC is strongly tied to the IMF orientation. The CDC's form due to the magnetic connection between the high-altitude geomagnetic field and the magnetosheath field. Where these fields are anti-parallel, a null-point is formed, embedded within a more extensive region of strong magnetic shear consistent with the expansive reconnection lines reported by Onsager et al. (2001). Such a configuration enabling simultaneous anti-parallel and component reconnection has also been reported by Trattner et al. (2004). This magnetic shear defines a current sheet bounding the geomagnetic field and enabling reconnection to transport plasma from the magnetosheath into the low field region of the magnetosphere. This accumulation of plasma resulting from the outflow from the reconnection site towards the converging dipolar geomagnetic field generates the diamagnetic cavity. Thus, the cavity develops, offset from the dipolar axis in the direction of the IMF in agreement, for example, with the recent results of Nykyri et al. (2011a), who report results from a cluster event in which the position of the CDC moves in accordance with a rotation of the IMF. This behavior is evidenced in the model results as shown in Fig. 2. For northward IMF, the cavity is located on the tailward edge of the converging geomagnetic field. The CDC then rotates clockwise with the IMF, generating CDC's on the dawn side for 90° IMF (shown here only for illustrative completeness), and on the dayside for southward IMF.

Not only does the IMF orientation play a crucial role in determining the location of the CDC, but it also effects the overall structure of the CDC. This is not so much a direct result of adjacent magnetic field orientations across the magnetospheric boundary, but rather due to the direction of the streaming magnetosheath plasma relative to the convective motion of the newly reconnected magnetic flux. Figure 3 illustrates the differences in geometry between the cases of strongly northward and strongly southward IMF. For a strongly southward IMF orientation, the reconnected flux tubes on the cusp-side of the x-line convect largely tailward, nearly parallel to the magnetosheath flow. Such is not the case for a strongly northward IMF. In this orientation, the reconnected flux tubes on the cusp-side of the x-line convect in the opposite direction of the streaming magnetosheath plasma. The result is a significantly larger CDC under Northward IMF conditions. Zhou et al. (2000) found a similar narrowing of the cusp under southward IMF conditions in agreement with Newell and Meng (1987), as well as a widening under northward IMF. The nature and geometry of this boundary is discussed in detail in the following sections.

3.2 Northward IMF

In this section we present simulation results for a strongly northward IMF orientation with a small positive B_y-component as defined by an IMF clock angle of 10° (IMF clock angle describes the deviation from the z-axis of the projection of the IMF into the x-z plane in a clockwise sense). This IMF orientation is chosen to include a small B_y-component simply to avoid the singular case of precisely Northward IMF which is highly unlikely in the physical system due to the dynamic nature of the interplanetary magnetic field. Plasma flow is initialized in the magnetosheath with $M_A \sim 0.5$. Resistivity is prescribed according to Eq. (3). We begin with an overview of the cusp region with emphasis on the CDC and its boundaries. We then discuss the boundaries in more detail.

3.2.1 Cusp overview

For northward IMF with clock angle of 10°, the null point is located on the tailward side of the converging dipolar field, offset slightly in the positive y-direction due to the positive y-component of the IMF. Figure 4 shows cuts of various plasma parameters in the noon-midnight meridian plane. The density (top left) and pressure (middle left) are enhanced (relative to the adjacent magnetosphere) within the cusp funnel. The density also shows significant variability (up to ∼50 % of typical CDC values) within the CDC. The enhanced current density (top right) indicating strong magnetic shear lies in the vicinity of the null-point, towards the minimum x-boundary in the plots. The plasma velocity (bottom) exhibits a clear field-aligned flow emanating from this region of enhanced current. The region of enhanced flow in the y-direction near

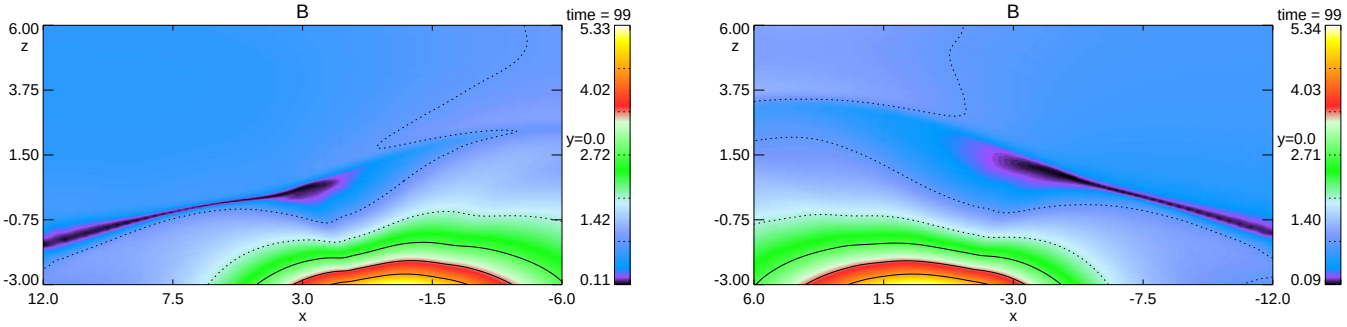

Fig. 3. Total magnetic field strength indicating diamagnetic regions plotted near the noon-midnight meridian plane for the cases of strongly southward IMF (left) and strongly northward IMF (right).

the maximum x-boundary in the figure is due to the reconnected magnetospheric field convecting under the specific IMF conditions. A region of high plasma β (middle right) is clearly visible extending cuspward from the current sheet. The location and extent of this high β region agree well with that of the depleted magnetic field shown in Fig. 3. These quantities both give reasonable indications of the CDC. The CDC is tilted anti-sunward (note the neglect of dipole tilt in the model) and is larger than for the southward case (discussed below).

Simulated "data" for a trajectory along z at $(x, y) = (-3.1, 0)$ in Fig. 4 through the high-altitude cusp region is shown in Fig. 5. The plot represents a traversal of the cusp region on the tailward edge of the cusp funnel. The transition from the strong dipolar field geometry accompanied by low density and plasma flow around $x = -.2\ R_E$, to a lower magnetic field strength and higher density with enhanced flow, indicates the inner boundary between the magnetosphere and CDC. The CDC region is easily identified through the characteristically large plasma β. The highlighted area in the figure represents the region within which the normalized plasma $\beta > 5$ (there is no significance in the value of β chosen here, the intention is simply to give an indication of the approximate location of the CDC). The CDC is a region of enhanced density and temperature relative to magnetospheric values. Within the CDC is a region of relatively low plasma flow with increasing convection and enhanced density towards the exterior of the CDC. The outer boundary between the CDC and magnetosheath is quite abrupt in comparison to the inner boundary. This is clearly evident as the flow rotates to align with the orientation of the streaming magnetosheath plasma concurrent with the magnetic field attaining IMF orientation.

Three boundaries are identified surrounding the CDC under northward IMF conditions: (1) the dayside plasma sheet/CDC boundary on the sunward side of the cusp, (2) the lobe/CDC boundary on the tailward side of the cusp, and (3) the CDC/magnetosheath boundary in the exterior. The following sections focus on the analysis of these boundaries.

3.2.2 Dayside plasma sheet/CDC boundary

The inner dayside plasma sheet/CDC boundary is identified by a very gradual decrease in temperature and increase in density occurring over a span of roughly 2 R_E. We were unable to find any intervals for this boundary which satisfied the Walén relation. This is not surprising, as it is not expected that this inner boundary represent an Alfvénic transition under northward IMF conditions. We were able to find good deHoffman-Teller frames for the inner transition with a typical velocity of $V_{HT} = (.02, -.01, -.02)$, indicating that the feature is steady-state. The sense and magnitude of convection is consistent with the expectations for flux convecting from a high-latitude reconnection site after having reached the inner boundary with the dayside plasma sheet.

3.2.3 Lobe/CDC boundary

The inner boundary between the lobe and CDC is a similarly gradual transition, marked largely by increasing density and plasma flow when traversing from the magnetospheric side. The transition is less gradual than the inner boundary on the dayside, spanning a distance of roughly 1 R_E. All traversals of the boundary yielded good deHoffman-Teller frames with typical velocities of $V_{HT} = (.2, .05, .2)$, indicating a convection away from the Earth and sunward, consistent with the expected convection for lobe reconnection. The boundary shows no indication of being Alfvénic in nature, as the Walén relation consistently yielded a slope of approximately $-.3$.

3.2.4 CDC/magnetosheath boundary

On exiting the CDC, the outer boundary with the magnetosheath is identified by the rotation of the magnetic field and plasma flow to magnetosheath values. This boundary is markedly more distinct than the inner boundaries. The boundary was analyzed at various locations yielding consistent deHoffman-Teller velocities and slopes of the Walén relation between .8 and 1.2. The deHoffman-Teller and Walén analyses are shown in Fig. 6 for a representative traversal at $(x, y) = (-5, 0)$.

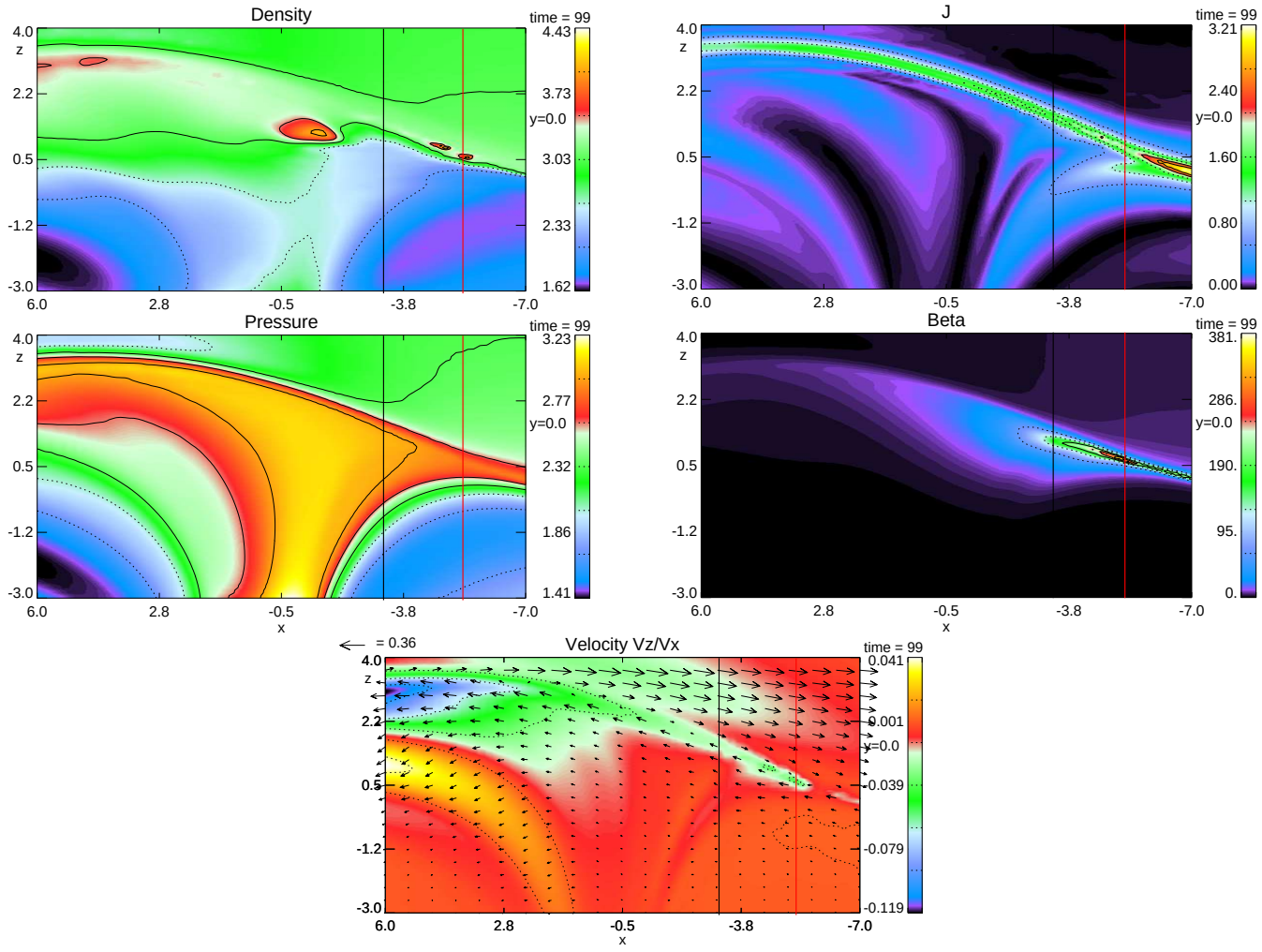

Fig. 4. From top to bottom, the plots on the left display plasma density, thermal pressure, and plasma velocity, while those on the right display current density (J) and plasma β. All parameters are shown in the noon-midnight meridian plane. The black and red vertical lines indicate the trajectories along which simulated data is analyzed in Sects. 3.2.1 and 3.2.4, respectively.

A good deHoffman-Teller frame is found with a velocity $V_{\rm HT} = (.09, -.07, .04)$. The slope of the Walén relation yields a value of 0.995 with corresponding correlation coefficient of 0.995, indicating that the boundary represents an Alfvénic transition resulting from lobe reconnection. MVA results are shown in Fig. 7. MVAE gives a max/int eigenvalue ratio of 53.06 with a normal eigenvector $i_{\rm E} = (-.33, .21, .92)$, while MVAB results in an int/min eigenvalue ratio of only 7.27. We therefore use the boundary normal coordinates determined through MVAE in the analysis of the discontinuity. The plasma data transformed in to MVAE coordinates are shown in Fig. 8. The interval which was analyzed is $\Delta z = 0.7 - 0.9$.

The normal components of the magnetic field and velocity are negative. This indicates that the boundary is open and plasma is being transported from the magnetosheath into the CDC. Additionally, the density and pressure increase, while the tangential magnetic field decreases. This transition then is mostly consistent with a slow shock. Note that the magnetic field is nearly completely turned off across the transition as would be the case for a switch-off slow shock, and thus the agreement with the Walén relation.

Normals resulting from MVA for the outer boundary were mostly oriented in the z-direction. The angle between normals computed for traversals of the outer boundary in the noon-midnight meridian plane at $x = -8\,R_{\rm E}$ and $-3\,R_{\rm E}$ is 17°, indicating that the outer boundary is indented in the x-z plane. Similar comparison for boundary normals along $x = -3\,R_{\rm E}$ at $y = 0\,R_{\rm E}$ and $3\,R_{\rm E}$ reveals that the boundary is convex between the two normals with an opening angle of 25°. A more detailed illustration of the geometry of this outer boundary is shown in Fig. 9. The CDC bulges outward toward the magnetosheath in the y-z plane (left), while tilted tailward and indented in the x-z plane (right).

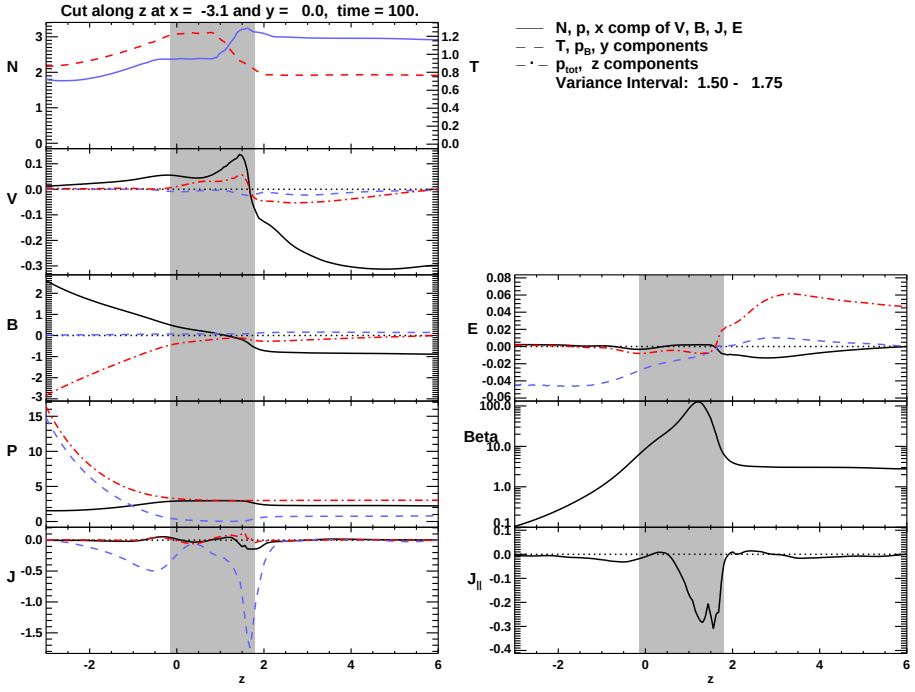

Fig. 5. Simulated data for a cut along z at $(x, y) = (-3.1, 0)$. All quantities are plotted in normalized simulation units. Plotted in the left column from top to bottom are the density (solid blue line) and temperature (dashed red line), velocity components (x – solid black, y – dashed blue, z – dash-dot red), magnetic field components, pressure (thermal pressure – black, magnetic pressure – blue, total pressure – red), and current density components. The right column displays (from top to bottom) the electric field components, plasma β, and the parallel current density. The shading indicates regions of plasma $\beta > 6$.

3.2.5 Discussion of northward IMF cusp

The high-altitude cusp region under northward IMF conditions may be summarized as follows. The inner boundaries of the cusp form a funnel shape and are seen as gradual (occurring over the span of 1–2 R_E) transitions in the density and temperature from typical magnetospheric values to those more comparable to the magnetosheath. This gradual nature of the inner lobe/CDC boundary under northward IMF conditions is in agreement observations (Lavraud et al., 2002; Nykyri et al., 2011a) however Lavraud et al. (2002) report a much more abrupt boundary between the dayside plasma sheet and CDC for the same IMF. The transition from the lobe is accompanied by increasing (largely field-aligned) flows on approach to the CDC region (see bottom plot in Fig. 4). These flows are qualitatively consistent with reports in the literature of field aligned flows along the inner boundary for northward IMF (Lavraud et al., 2004b, 2005; Dunlop et al., 2005; Nykyri et al., 2011a), though the results presented herein indicate significantly smaller flows. It should be noted, however, that the density asymmetry (between the magnetosphere and the magnetosheath) is rather small in this configuration, characterized by a change of only a factor of ∼1.5. Simulations with a more physical density distribution (realizing a change in density by a factor of ∼50) and a higher resolution (however, a somewhat shorter physical duration) indicate parallel flows a factor of three larger than the bulk velocity in the CDC. Within the CDC, flows are significantly more moderate (60 km s^{-1}), in agreement with the stagnant exterior cusp (SEC) reported by Lavraud et al. (2002).

The exterior CDC/magnetosheath boundary is much more abrupt than the inner boundaries. The outer boundary is indented in the x-z plane, but is convex in the y-z plane. Analysis of the outer boundary reveals an Alfvénic transition (indicated by the slope of the Walén relation of 0.995 with c.c. = 0.995). The plasma parameters change in a manner mostly consistent with a slow-shock, often associated with reconnection.

3.3 Southward IMF

In this section we present simulation results for a strongly southward IMF orientation with IMF clock angle of 170°, resulting in a B_y-component identical to that for the northward case. Plasma flow for the southward case is initialized in the magnetosheath region with $M_A \approx 1$, while the resistivity is identical to the northward case (defined through Eq. 3). We begin with an overview of the cusp region with emphasis on the CDC and its boundaries. We then discuss the boundaries in more detail, following the same format as in the previous section for northward IMF.

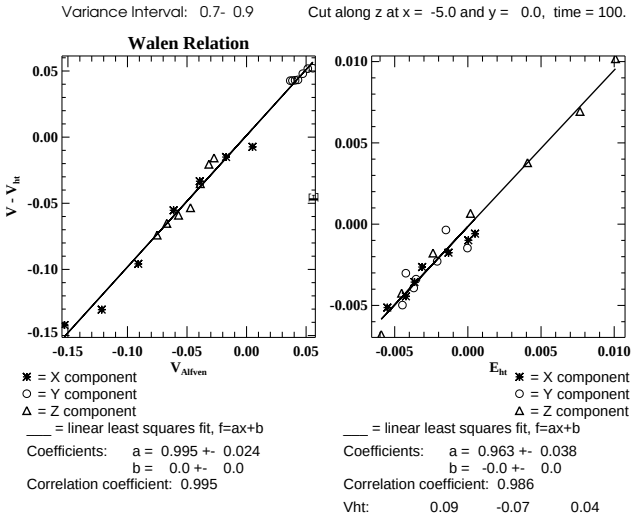

Fig. 6. Walén relation (left) and deHoffman-Teller test (right) results for the CDC/magnetosheath boundary for the interval $z = [0.7-0.9]$ at $(x, y) = (-5, 0)$.

3.3.1 Cusp overview

For an IMF orientation of 170°, the CDC looks quite different from the northward IMF configuration. An IMF clock angle of 170° generates a null-point on the dayside of the cusp, slightly offset in the positive y-direction (duskward). Figure 10 shows cuts of various plasma parameters in the noon-midnight meridian plane. The density (top left) and pressure (middle left) are enhanced (relative to the adjacent magnetosphere) within the cusp funnel. The enhanced current density (top right) indicating strong magnetic shear lies in the vicinity of the null-point, towards the maximum x-boundary in the plots. The plasma velocity (bottom) exhibits a clear field-aligned flow emanating from this region of enhanced current. A region of high plasma β (middle right) is clearly visible extending cuspward from the current sheet. The location and extent this high β region agree well with that of the depleted magnetic field shown in Fig. 3. The CDC is tilted sunward (note the neglect of dipole tilt in the model) and is significantly smaller than for the northward case. The cuspward directed outflow from the reconnection site adjacent to the boundary with the magnetosheath is nearly parallel to the streaming magnetosheath flow. The newly reconnected magnetospheric field line is thus rapidly transported from the dayside, tailward, resulting in a relatively small CDC. The overall CDC is rather shallow, extending just over 1 R_E along the z-direction at its deepest extent into the cusp funnel, extending well past the central cusp region in a thin tailward structure compatible with the Cluster results for southward IMF cusp structure (Cargill et al., 2004). In comparison, the CDC for the northward case shown in Fig. 3 extends just more than 2 R_E along the z-direction. These results are consistent with reports of a smaller cusp under southward IMF conditions as evidenced by Cluster traversal of the high-altitude cusp region (Cargill et al., 2004) as well as mid-altitude cusp precipitation (Escoubet et al., 2008).

Simulated "data" for a trajectory along z at $(x, y) = (3, 0)$ in Fig. 10 through the high-altitude cusp region is shown in Fig. 11. The displayed "data" represents a cut through the dayside edge of the cusp region at $x = 3\,R_E$. The dayside plasma sheet is evident from $z = -4\,R_E$ until just above $z = -2\,R_E$. This is indicated by the typical low density and plasma velocity, but strong, dipolar magnetic field geometry. Strong plasma flows are present near $z = -1\,R_E$, along with increased density and a current sheet indicating the departure from a dipolar magnetic field geometry. The plasma flow in this layer has a significant field-aligned component, consistent with outflow from sub-solar reconnection. The CDC "proper" lies adjacent to this layer of strong plasma flow as indicated by the shaded region of large plasma β in the figure. The CDC is relatively shallow at this location, spanning a distance on the order of .5 R_E. The CDC is bounded in the exterior by a clear transition to magnetosheath plasma values.

We identify three boundaries of the CDC for southward IMF: (1) the dayside plasma sheet/CDC boundary on the sunward side of the cusp, (2) the lobe/CDC boundary on the tailward side of the cusp, and (3) the CDC/magnetosheath boundary in the exterior. The following sections focus on the analysis of these boundaries.

3.3.2 Dayside plasma sheet/CDC boundary

The inner boundary between the dayside plasma sheet and the CDC is clearly identified by the deviation of the magnetic field (specifically B_x, B_y) from its dipolar geomagnetic values. We were able to find good a deHoffman-Teller frame (slope of 1.00 with c.c. = 0.957) for the inner boundary with a velocity (in normalized units) of $V_{HT} = (-.49, .08, -.18)$. This indicates that the structure is convecting largely tailward and towards the Earth, but with a small duskward component, consistent with a dayside reconnection site. Plots of the deHoffman-Teller and Walén tests are displayed in Fig. 12.

The transition from the dipolar geomagnetic field to the reduced diamagnetic region spans a much larger interval than the one analyzed above and generally does not satisfy the Walén relation. However, the interval analyzed above is mostly consistent with an Alfvénic transition, though the results are strongly dependent on the chosen interval. The positive result for the Walén relation shown in Fig. 12 may be due to the interval of analysis not spanning the entire transition. There is evidence that this boundary may be a tangential discontinuity (TD) under northward IMF conditions (Cargill et al., 2005, for instance), however this may not be the case for southward IMF. Under southward IMF, this transition which appears Alfvénic in the simulation may indeed be a reconnection associated shock extending form the reconnection site at the magnetopause towards the cusp funnel

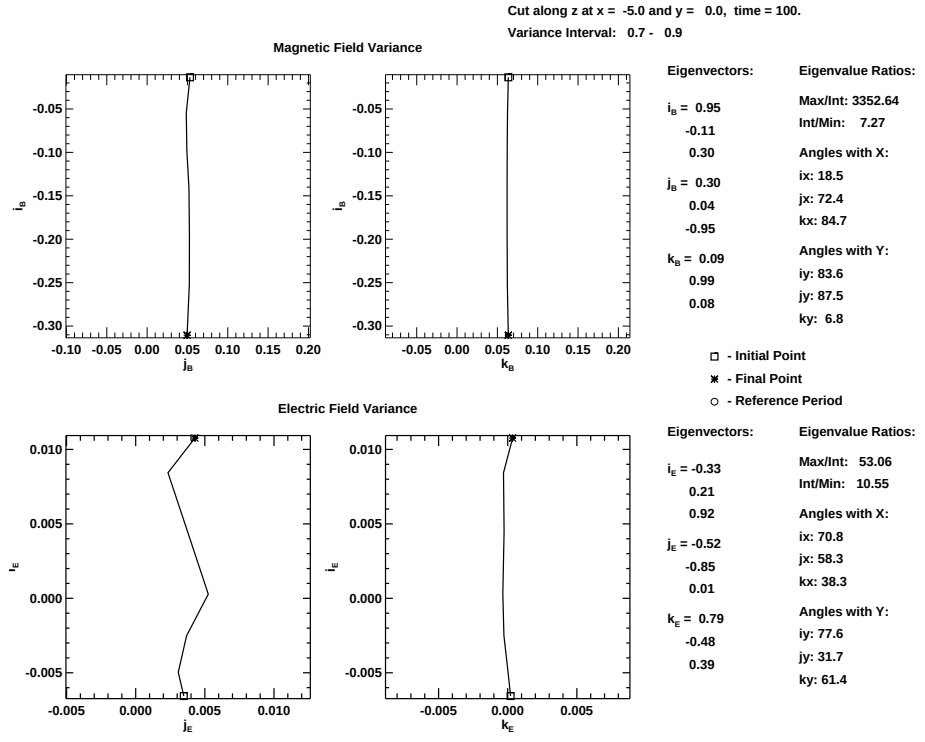

Fig. 7. Results of the boundary normal calculation for the traversal of the CDC/magnetosheath boundary at $(x, y) = (-5, 0)$ under northward IMF conditions.

along the bottom edge of the CDC. Such a configuration would be reminiscent of the shocks in the Petschek model (Petschek, 1964), but in a highly asymmetric configuration wherein the transition appears as a slow shock in the vicinity of the reconnection site, while farther away it appears more like a tangential discontinuity. Higher resolution in future work may allow for a more detailed analysis.

MVAB resulted in poor intermediate to minimum eigenvalue ratios (int/min = 3.26). Results of MVAE were better, with a maximum to intermediate ratio of 76.29, though the resolution of the transverse components remains ambiguous (int/min: 3.26). The boundary normal given by MVAE is $i_{\mathrm{E}} = (-.01, -.23, .97)$. The simulated data (transformed into the basis resulting from MVAE) is plotted in Fig. 13. In the framework of ideal MHD discontinuities, the increase in pressure from the magnetospheric side of the boundary towards the CDC implies the existence of a shock through which plasma is transported in the same sense as indicated by the positive normal component of the flow in the deHoffman-Teller frame (upper panel in the right of the figure). The concurrent variation of the magnetic field and velocity are suggestive of a slow-shock, though the normal component of the magnetic field decreases, inconsistent with the expectation for such a structure. This may be the result of inaccurate basis given by the MVAE method, or it may be that the gradual nature of the inner boundary in the simulation renders its classification as an ideal MHD discontinuity invalid.

3.3.3 Lobe/CDC boundary

The inner boundary between the magnetospheric lobe and the CDC is a gradual and continuous transition marked largely by the slow transition from the dipolar geomagnetic field to the depressed field of the CDC region. This transition is similar to the inner boundary on the dayside as addressed in the previous section, but even more gradual spanning an interval of roughly 2 R_{E}. No regions were found through which this boundary could be approximated as an MHD discontinuity, and thus no boundary analysis is presented here. This region is marked by steadily decreasing magnetic field on approach to the CDC from below, along with increasing plasma flow, while the density and thermal pressure remain relatively constant, consistent with the plasma mantle (Rosenbauer et al., 1975).

3.3.4 CDC/magnetosheath boundary

The outer boundary between the CDC and the magnetosheath is most easily identified by the change in magnetic field from low CDC values to IMF values. Analysis of this exterior boundary at different locations along the noon-midnight meridian, both sunward and tailward of the cusp funnel, results in good deHoffman-Teller frames, moving largely in the $-$x and $+$z directions, consistent with tailward convection due to reconnection occurring on the dayside.

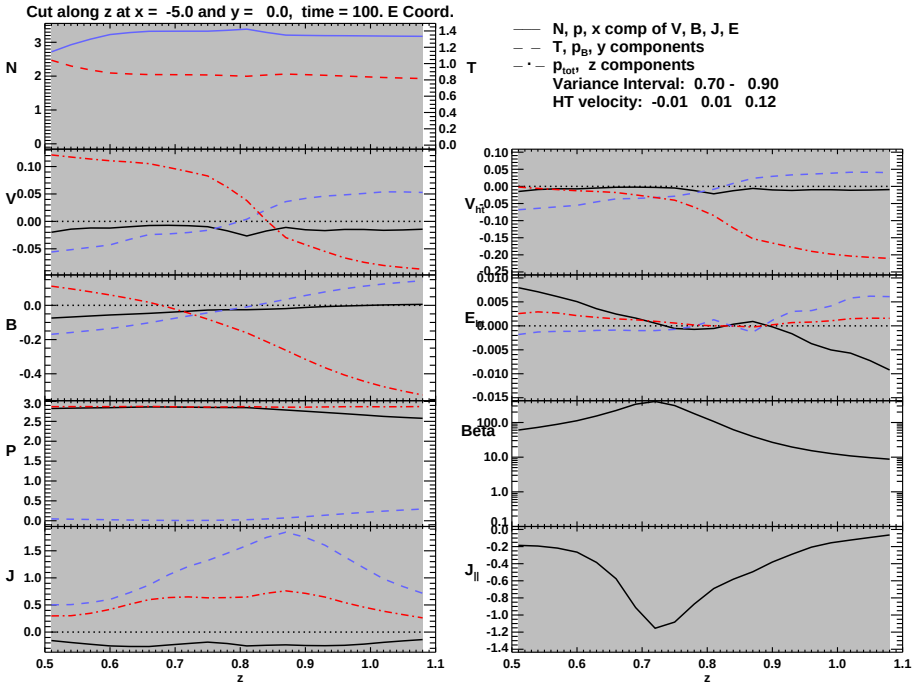

Fig. 8. Simulated "data" for a cut along z at $(x,y) = (3,0)$ transformed into MVAE boundary normal coordinates for outer CDC/magnetosheath boundary. All quantities are plotted in normalized simulation units. Plotted in the left column from top to bottom are the density (solid blue line) and temperature (dashed red line), velocity components (x – solid black, y – dashed blue, z – dash-dot red), magnetic field components, pressure (thermal pressure – black, magnetic pressure - blue, total pressure – red), and current density components. The right column displays the velocity and electric field components in the deHoffman-Teller frame, plasma β, and the parallel current density.

Searches were performed to identify intervals within which the Walén relation achieved a slope of between 0.85 and 1.15, while the slope of the deHoffman-Teller electric field versus the electric field in the simulation frame was between .90 and 1.1. In general, the outer boundary satisfies the Walén relation within the range previously stated. For the boundary crossing at $x = 3$, the slopes of the deHoffman-Teller and Walén tests were .993 and 1.035, respectively, with corresponding correlation coefficients of 0.997 and .991. The deHoffman-Teller velocity was found to be $V_{\rm HT} = (-.34, -.07, .10)$. The boundary normal resulting from MVAE was $i_{\rm E} = (.15, .52, .84)$. The plasma parameters transformed into this frame are plotted in Fig. 14.

The normal components of both the velocity and magnetic field are negative, indicating an open boundary through which plasma is transported from the magnetosheath into the CDC. Variation of the remaining plasma parameters is consistent with a slow-shock: pressure increase, decrease in transverse components of magnetic field and velocity, and temperature increase. This indicates that the boundary is formed by reconnection processes at the magnetopause.

MVA resulted in normals with largest components aligned with the y- and z-directions. Comparison of normals given by MVAE for the boundary at $x = 5$ and $x = 2.8$ and projected into the x-z plane reveals that the boundary farther away from the reconnection site ($x = 2.8$) is oriented 25° towards the sun from the normal computed at $x = 5$. This indicates a clear indentation of the outer boundary under these IMF conditions. Similar analysis of boundary normals at $y = 0$ and $y = 1$, reveals that the computed normals open with an angle of 35° from each other. This indentation of the outer boundary is clearly visible in Fig. 15. The figure displays the total magnetic field in the y-z (top) and x-z (bottom) planes.

3.3.5 Discussion of southward IMF cusp

The high-altitude cusp region is bounded by two gradual inner boundaries with the magnetosphere. These boundaries form a definite funnel shape (as for the northward case presented above). Though the inner boundaries are quite gradual, we were able to find an interval for the crossing of the inner CDC/dayside plasma sheet boundary which reasonably well satisfied the Walén relation (slope of $-.805$ with c.c. = .968). Excluding the decrease in the normal component of the magnetic field (which may be the result of a poor normal determination), this transition is mostly consistent with a slow-shock. We note, however, that the gradual appearance of the transition from the dipolar geomagnetic field to the reduced diamagnetic region spans a much larger interval than the one analyzed above and it generally does not satisfy the

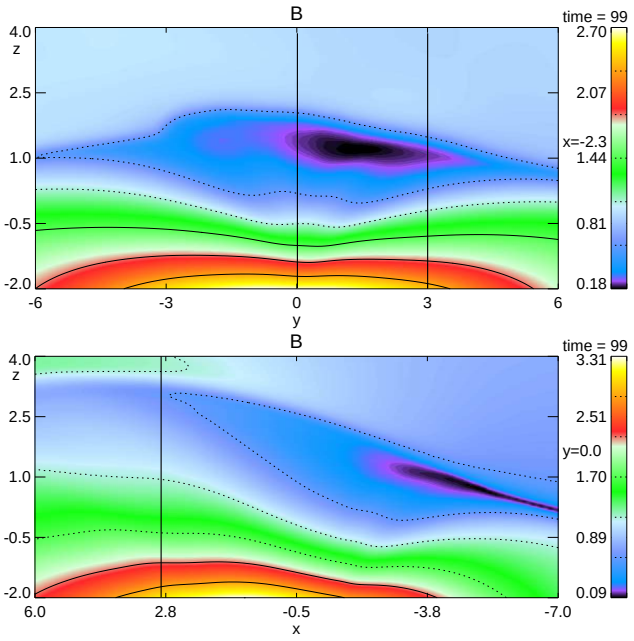

Fig. 9. Total magnetic field ($|B|$) in the y-z plane (top), and x-z plane (bottom) for northward IMF. The CDC region is indicated by low magnetic field magnitude. The boundary normals used to address the geometry of the outer boundary are computed approximately along the vertical lines in the figures (note that the cut at $x = -8\,R_E$ is not shown in the lower plot).

Walén relation. This gradual nature of the inner boundary in the simulation may simply render its classification as an ideal MHD discontinuity invalid.

The CDC for southward IMF is filled with streaming plasma similar to that reported by Cargill et al. (2004) and Lavraud et al. (2005), as opposed to the results for northward IMF with a stagnant region (Lavraud et al., 2002, 2005). This is not unexpected, due to the plasma flow in the sheath streaming in the same sense as the reconnected flux.

The outer CDC/magnetosheath boundary is much more abrupt than the inner boundaries and is indented in both the x-z and y-z planes. The boundary appears to be open (indicated by the $-B_n$) implying plasma transport from the magnetosheath into the CDC. The plasma characteristics across the boundary are consistent with a slow-shock suggesting that reconnection is the dominant process in the development of this boundary.

4 Discussion and conclusion

We have presented results from local meso-scale resistive MHD simulations which address the effects of variations in the IMF orientation on the high-altitude cusp region. Typical observational features of CDC's are generally well reproduced in the simulation results:

1. Densities comparable to magnetosheath values
2. Strongly depressed magnetic field strength
3. Relatively stagnant plasma for northward IMF, but more convective flow for southward IMF
4. Gradual inner boundaries with a more abrupt boundary with the magnetosheath.

The high-altitude cusp has three boundaries: (1) the inner dayside plasma sheet boundary, (2) the inner lobe/mantle boundary, and (3) the outer magnetosheath boundary. The inner boundaries appear in the simulation as gradual transitions which exhibit field-aligned flows emanating from the side of the cusp where reconnection is occurring: the dayside plasma sheet boundary for southward IMF and the lobe boundary for northward IMF. The gradual appearance of the inner boundaries further supports the suggestion that it is appropriate to view the high-altitude cusp region containing the CDC and SEC as an extension of the magnetosphere (Russell, 2000; Lavraud et al., 2004b), and not as a detached structure as implied by the term "exterior".

Though the above features are reasonably well in agreement with observations, there remain a few aspects of the model results which disagree with some observational reports. These have to do with the inner boundaries between the magnetosphere and the CDC and with the presence of magnetic fluctuations within the CDC's.

The inner boundaries between the magnetosphere and CDC are represented by gradual transitions in the model. Though some observations agree with this gradual character for the inner transitions, for example Niehof et al. (2010); Nykyri et al. (2011a), others describe a much more rapid transition (Lavraud et al., 2002). This may be partly due to the dynamic nature of the cusp region, for instance Nykyri et al. (2011b) have shown that some of the local fluctuations in plasma parameters within the CDC may be attributed to the reaction of the CDC to solar wind changes on relatively short timescales. This gradual transition in the simulation may also be caused by limited resolution (note that the simulation already has a much higher resolution than typical global models) or by physics not contained within our model such as dipole tilt or inherent fluctuations within the solar wind plasma. These inner boundaries also exhibit significant field-aligned flows. These flows as seen in the simulation results, though qualitatively consistent with observations (Lavraud et al., 2004b, 2005; Dunlop et al., 2005; Nykyri et al., 2011a) are relatively small. It was previously noted that this appears to be the result of the low density asymmetry (between the magnetosphere and the magnetosheath) in this configuration. Simulations with a more physical density distribution and a higher resolution indicate parallel flows a factor of three larger than the bulk velocity in the CDC.

The other characteristic of CDC's that is not well represented in the model is the presence of magnetic fluctuations

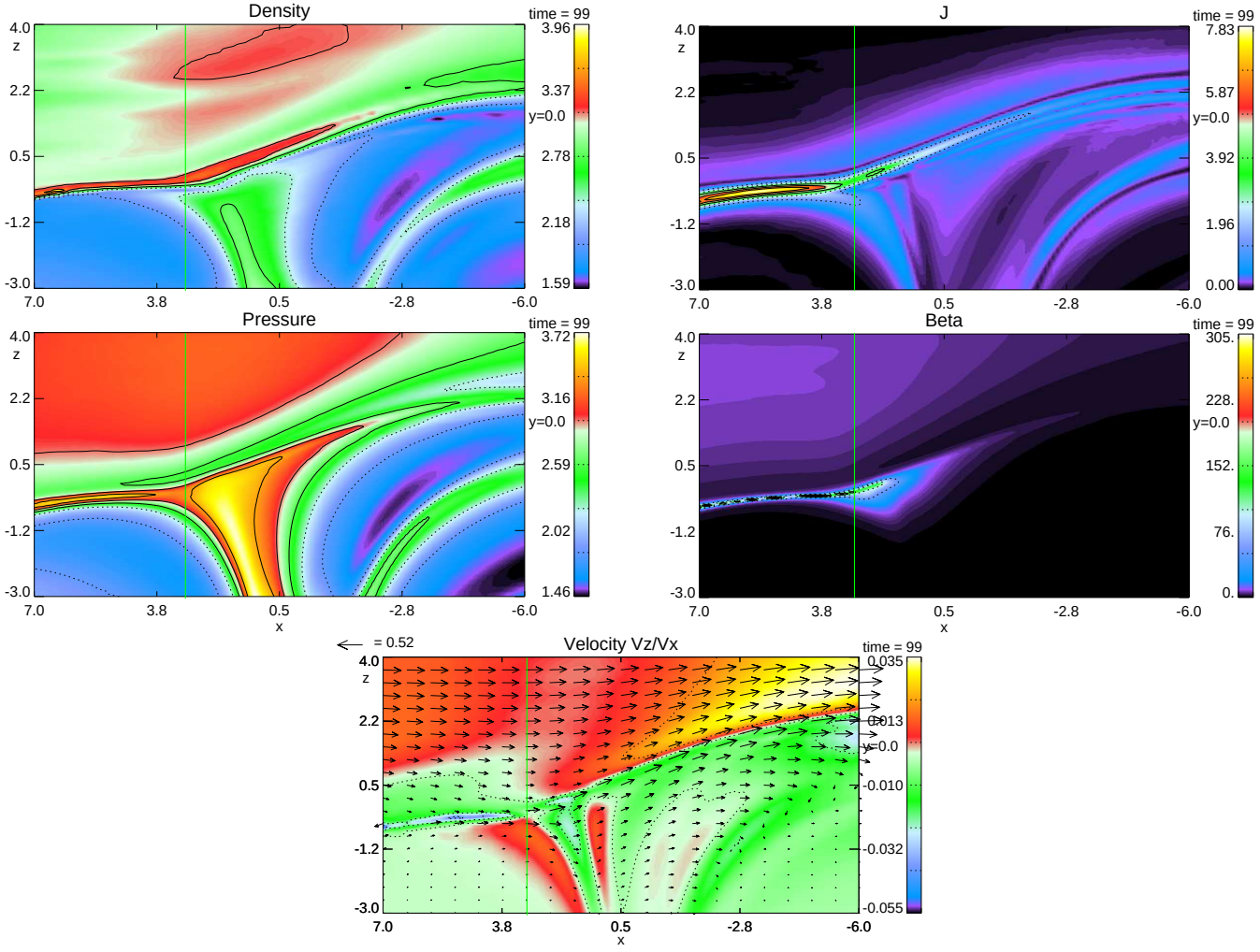

Fig. 10. From top to bottom, the plots on the left display plasma density, thermal pressure, and plasma velocity, while those on the right display current density (J) and plasma β. All parameters are shown in the noon-midnight meridian plane. The green vertical lines indicate the trajectories along which simulated data is analyzed.

such as those reported by Chen and Fritz (1998). The nature and cause of these fluctuations remains unclear in the observations and they may be the result of several processes such as rapid motion of cavity boundaries, transient events, such as magnetic flux bundles moving along the cavity, or waves within the region. It is possible that the consideration of such inputs in the model may indeed explain the observed fluctuations, however that is beyond the scope of this paper.

The main conclusions of this work may be summarized as follows:

1. Both the location and extent of the CDC exhibits a strong dependence on the IMF orientation. Results suggest that the extent of the high-altitude cusp, farthest from the dipole axis along the magnetopause, is anchored to the magnetopause through magnetic merging at the location of strongest magnetic shear. For northward IMF, the cusp is situated tailward of the dipole axis. Conversely, for southward IMF, the cusp is located on the sunward side of the dipole axis. Similar results were shown, though not discussed in detail, for the case of 90° clock angle in Fig. 2. These results are in agreement with the recent results of Nykyri et al. (2011a), who report results from a cluster event in which the position of the CDC moves in accordance with a rotation of the IMF.

The CDC appears significantly larger under northward IMF conditions than for southward IMF conditions. For a strongly southward IMF orientation, the reconnected flux tubes on the cusp-side of the x-line convect largely tailward, nearly parallel to the magnetosheath flow. Such is not the case for a strongly northward IMF. In this orientation, the reconnected flux tubes on the cusp-side of the x-line convect in the opposite direction of the streaming magnetosheath plasma. The result is a

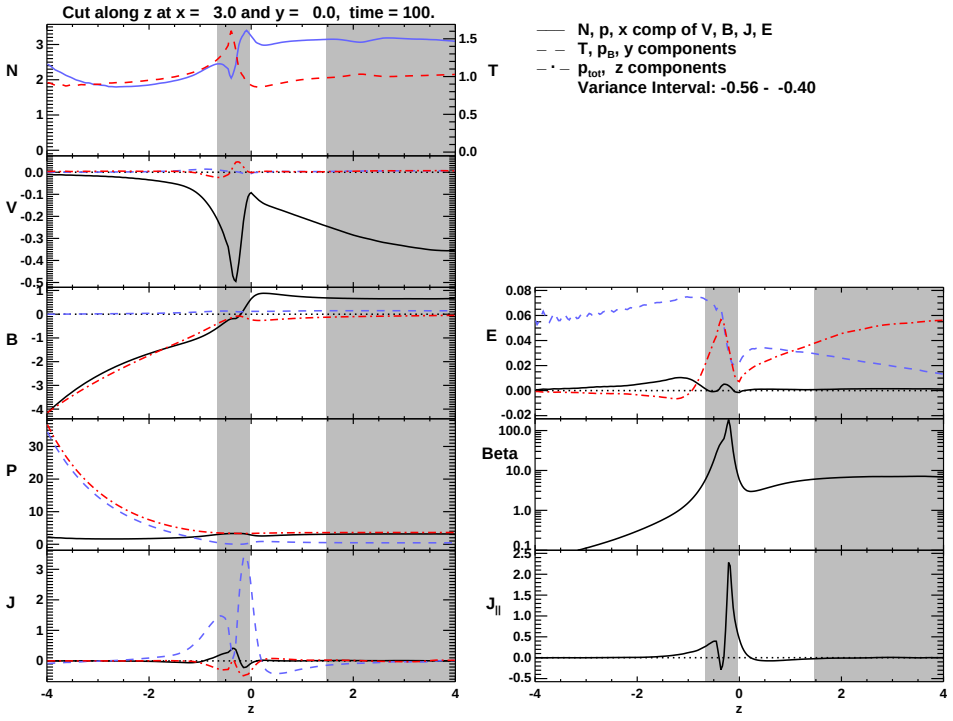

Fig. 11. Simulated data for a cut along z at $(x, y) = (3, 0)$. All quantities are plotted in normalized simulation units. Plotted in the left column from top to bottom are the density, velocity components, magnetic field components, pressure, and current density. The right column displays the electric field, plasma β, and the parallel current density. The shading indicates regions of plasma $\beta > 6$.

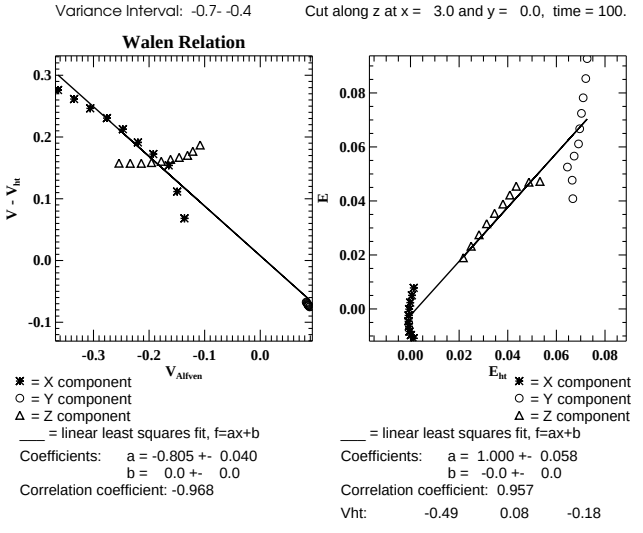

Fig. 12. Walén relation and deHoffman-Teller test results for the dayside plasma sheet/CDC.

significantly larger CDC under Northward IMF conditions. Zhou et al. (2000) found a similar narrowing of the cusp under southward IMF conditions in agreement with Newell and Meng (1987), as well as a widening under northward IMF.

2. The location of the reconnection site is determined by the orientation of the IMF. Where the geomagnetic field and the IMF are anti-parallel, a null-point is formed, embedded within a more extensive region of strong magnetic shear consistent with the expansive reconnection lines reported by Onsager et al. (2001). Such a configuration, enabling simultaneous anti-parallel and component reconnection has also been reported by Trattner et al. (2004).

3. The outer boundary between the CDC and magnetosheath appears mostly consistent with a slow-shock. Transformation of the plasma parameters near the boundary into the coordinate system defined through MVA methods applied to our simulation results indicate a boundary characterized by a negative normal component of both the magnetic field and velocity, accompanied by an increase in pressure and density, and a reduction in the tangential components of the magnetic field and velocity. The normal components of the magnetic field and velocity across the transition indicate an open boundary across which plasma is transported from the magnetosheath to the CDC. Similar open boundaries have been reported in case studies by Cargill et al. (2004) under southward IMF conditions and by Lavraud et al. (2002, 2004b) for northward IMF. The jump in plasma parameters across the transition are suggestive

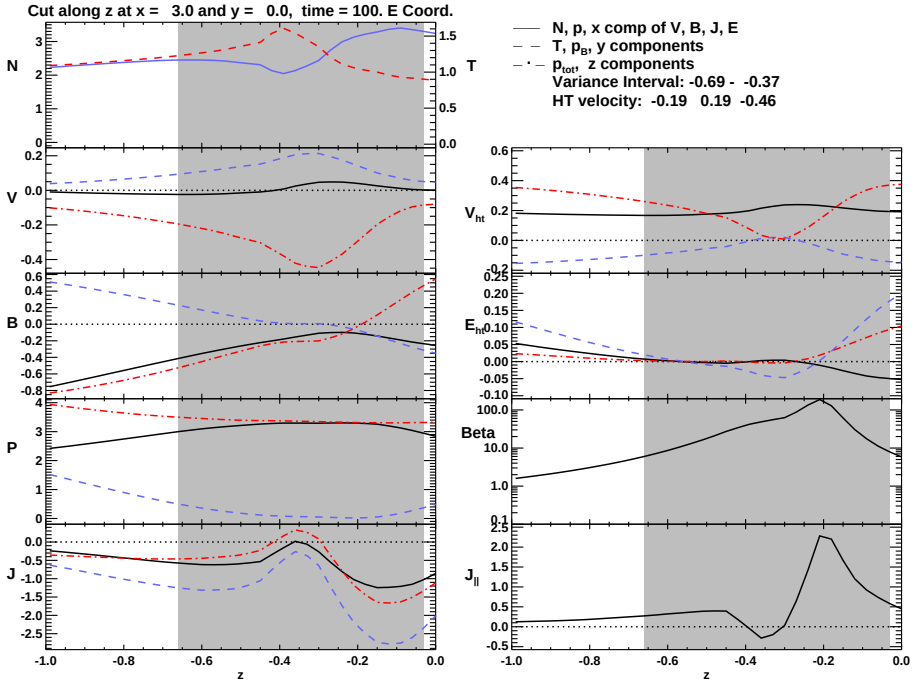

Fig. 13. Simulated "data" transformed into MVAE boundary normal coordinates for the inner boundary transition. All quantities are plotted in normalized simulation units. Plotted in the left column from top to bottom are the density (solid blue line) and temperature (dashed red line), velocity components (x – solid black, y – dashed blue, z – dash-dot red), magnetic field components, pressure (thermal pressure – black, magnetic pressure – blue, total pressure – red), and current density components. The right column displays the velocity and electric field components in the deHoffman-Teller frame, plasma β, and the parallel current density.

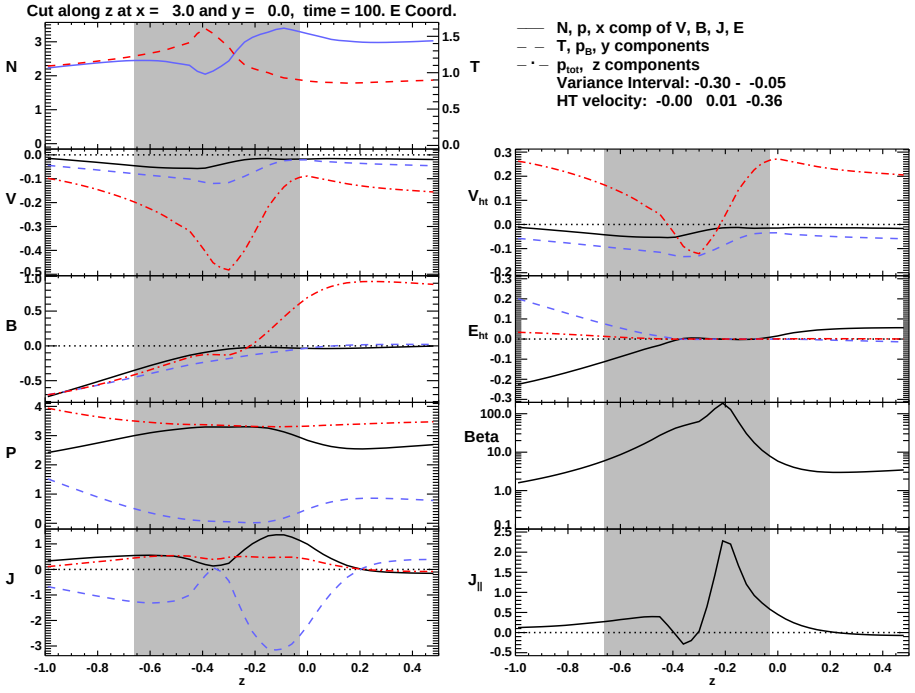

Fig. 14. Plasma parameters transformed into the basis given by MVAE for the outer boundary between the CDC and magnetosheath at $x = 2.1$.

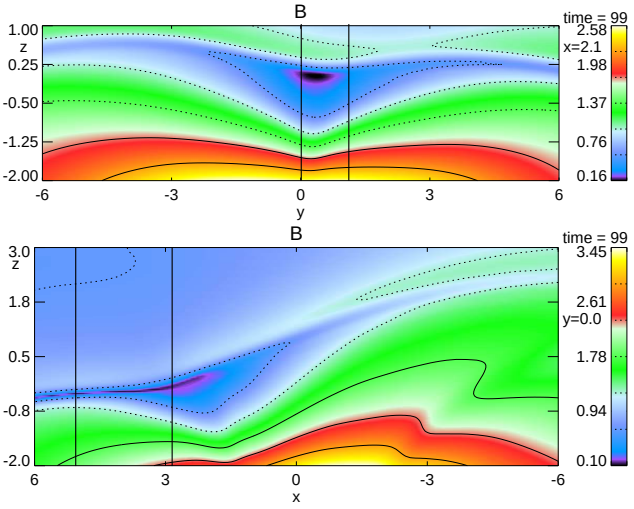

Fig. 15. Total magnetic field ($|B|$) in the y-z plane (top), and x-z plane (bottom) for southward IMF. The CDC region is indicated by low magnetic field magnitude. The boundary normals used to address the geometry of the outer boundary are computed approximately along the vertical lines in the figures.

of a slow shock. However, unexpectedly for a slow shock, the Walén test is well satisfied for the transition. Similar results were reported by Lavraud et al. (2002) and Cargill et al. (2004) for northward and southward IMF, respectively. Lavraud et al. (2002) found a value of .91 for the Walén relation, but noted that the change in plasma parameters was not consistent with a simple rotational discontinuity. They suggest that the boundary, though rotational-like, may be an intermediate or slow transition. Similarly, the results of Cargill et al. (2004) indicate a good value of the Walén relation of .8, but again note that the plasma parameter jumps across the boundary are inconsistent with a simple RD. They note that some characteristics of the transition are satisfied for a number of MHD discontinuities, however no simple discontinuity can explain them all. For instance, the good Walén relation is largely consistent with a rotational discontinuity, but such a transition does not exhibit the observed magnetic field and temperature changes. The authors also note that the parameter jumps are largely consistent with a slow shock if the Alfvénic character is neglected. We note that this apparent dual nature (Alfvénic and slow-shock like) may be explained in our simulation results through the fact that the tangential components of the magnetic field are nearly switched-off, whereas the Walén relation is approximately satisfied for switch-off slow shocks suggesting that magnetic reconnection is the dominant process in structuring this boundary.

4. We find the geometry of the magnetopause bounding the high-altitude cusp to differ based on IMF orientation. For northward IMF, the magnetopause exhibits an indentation in the x-z plane, but is convex in the y-z plane, whereas, the magnetopause appears indented in both x-z and y-z planes for southward IMF conditions. Numerous studies have presented evidence for an indented magnetopause (Eastman et al., 2000; Dunlop et al., 2005; Zhang et al., 2007), while others have identified no evidence for such a geometry (Zhou and Russell, 1997; Lavraud et al., 2004a; Cargill et al., 2004). Our results exhibit clear indentation of the magnetopause bounding the high altitude cusp with the magnetosheath, with the exception of the y-z plane under northward IMF conditions which appears convex. In a statistical study Zhang et al. (2007) report an external cusp boundary which is clearly indented in the x-y plane, but less clearly indented in the x-z plane. It is unclear exactly how our results are to be interpreted in terms of such observations due to the neglect of dipole tilt in our model. It is plausible that the consideration of dipole tilt in the model could alter the geometry of the magnetopause adjacent to the high-altitude cusp as the result of increased normal flow. In addition, results presented herein have considered sub-Alfvénic magnetosheath flow, whereas flow in the magnetosheath frequently realizes super-Alfvénic speeds. Consideration of magnetosheath flow with $M_A > 1$ may significantly alter results, particularly in terms of the geometry of the outer boundary. It is expected that the additional consideration of such effects would lead to further indentation of the magnetopause in the region (and thus possibly result in similar results also in the y-z plane under northward IMF). Thus our findings clearly support the existence of an indented magnetopause bounding the high altitude cusp region.

Our results paint a picture of the CDC as an attached feature of the high altitude cusp region, bounded on its exterior with the magnetopause. The magnetopause in the vicinity of the CDC appears Alfvénic in nature and exhibits characteristics consistent with a slow shock (nearly a switch-off slow shock). Additionally, the CDC exhibits a clear dependence on the IMF both in terms of its size and its location. These results suggest that the region is largely structured by reconnection processes (through concurrent anti-parallel and component merging) at the magnetopause largely under the control of the IMF. With evidence mounting for the role played by reconnection in forming this outer boundary, it may be more appropriately regarded as the magnetopause (Onsager et al., 2001; Lavraud et al., 2004b; Cargill et al., 2004), whereas the more gradual inner boundaries, as noted by Lavraud et al. (2004), appear more consistent with the traditional magnetopause (Paschmann et al., 1976; Haerendel et al., 1978; Russell, 2000).

Acknowledgements. Support for the research of Eric Adamson and Antonius Otto was provided by NASA grants NNG06GG89Gprog07 and NNX09AI09Gprog2010 to the University of Alaska Fairbanks. K. Nykyri's work is supported by National Science Foundation grant 0703327.

The service charges for this open access publication have been covered by the Max Planck Society.

Topical Editor R. Nakamura thanks J. Niehof and another anonymous referee for their help in evaluating this paper.

References

Adamson, E., Otto, A., and Nykyri, K.: 3-D mesoscale MHD simulations of a cusp-like magnetic configuration: method and first results, Ann. Geophys., 29, 759–770, doi:10.5194/angeo-29-759-2011, 2011.

Bosqued, J. M., Escoubet, C. P., Frey, H. U., Dunlop, M., Berchem, J., Marchaudon, A., Cerisier, J. C., Fazakerley, A., Budnik, E., Lavraud, B., Rème, H., Laakso, H., and Balogh, A.: Multipoint observations of transient reconnection signatures in the cusp precipitation: A Cluster-IMAGE detailed case study, J. Geophys. Res., 110, A03219, doi:10.1029/2004JA010621, 2005.

Carbary, J. F. and Meng, C. I.: Relations between the interplanetary magnetic field B_Z, AE index, and cusp latitude, J. Geophys. Res., 91, 1549–1556, 1986.

Cargill, P. J., Dunlop, M. W., Lavraud, B., Elphic, R. C., Holland, D. L., Nykyri, K., Balogh, A., Dandouras, I., and Rème, H.: CLUSTER encounters with the high altitude cusp: boundary structure and magnetic field depletions, Ann. Geophys., 22, 1739–1754, doi:10.5194/angeo-22-1739-2004, 2004.

Cargill, P. J., Lavraud, B., Owen, C. J., Grison, B., Dunlop, M. W., Cornilleau-Wehrlin, N., Escoubet, C. P., Paschmann, G., Phan, T. D., Rezeau, L., Bogdanova, Y., and Nykyri, K.: Cluster at the Magnetospheric Cusps, Space Sci. Rev., 118, 321–366, doi:10.1007/s11214-005-3835-0, 2005.

Chen, J. and Fritz, T. A.: Correlation of cusp MeV helium with turbulent ULF power spectra and its implications, Geophys. Res. Lett., 25, 4113–4116, doi:10.1029/1998GL900122, 1998.

Chen, J., Fritz, T. A., Sheldon, R. B., Spence, H. E., Spjeldvik, W. N., Fennell, J. F., Livi, S., Russell, C., Pickett, J. S., and Gurnett, D. A.: Cusp energetic particle events: Implications for a major acceleration region of the magnetosphere, J. Geophys. Res., 103, 69–78, 1998.

Dubinin, E., Skalsky, A., Song, P., Savin, S., Kozyra, J., Moore, T. E., Russell, C. T., Chandler, M. O., Fedorov, A., Avanov, L., Sauvaud, J.-A., and Friedel, R. H. W.: Polar Interball Coordinated Observations of Plasma and Magnetic Field Characteristics in the Regions of the Northern and Southern Distant Cusps, J. Geophys. Res., 107, 1053, 2002.

Dunlop, M. W., Lavraud, B., Cargill, P., Taylor, M. G. G. T., Balogh, A., Reme, H., P., D., Glassmeier, K.-H., Elphic, R. C., Bosqued, J. M., Fazakerley, A., Dandouras, I., Escoubet, C. P., Laasko, H., and Marchaudon, A.: Cluster Observations of the Cusp: Magnetic Structure and Dynamics, Springer Netherlands, 2005.

Eastman, T. E., Boardsen, S. A., Chen, S. H., Fung, S. F., and Kessel, R. L.: Configuration of high-latitude and high-latitude boundary layers, J. Geophys. Res., 105, 23221–23238, 2000.

Escoubet, C. P. and Bosqued, J. M.: The influence of IMF-B_Z and/or AE on the polar cusp: An overview of observations from the AUREOL-3 satellite, Planet. Space Sci., 37, 609–626, 1989.

Escoubet, C. P., Berchem, J., Bosqued, J. M., Trattner, K. J., Taylor, M. G. G. T., Pitout, F., Laasko, H., Masson, A., Dunlop, M., Dandouras, I., Rème, H., Fazakerley, A. N., and Daly, P.: Effect of a northward turning of the interplanetary magnetic field on cusp precipitation as observed by Cluster, J. Geophys. Res., 113, A07S13, doi:10.1029/2007JA012771, 2008.

Fedorov, A., Dubinin, E., Song, P., Budnik, E., Larson, P., and Sauvaud, J.-A.: Characteristics of the Exterior Cusp for Steady Southward Interplanetary Magnetic Field: Interball Observations, J. Geophys. Res., 105, 15945–15957, 2000.

Fritz, T. A., Chen, J., and Siscoe, G. L.: Energetic ions, large diamagnetic cavities, and Chapman-Ferraro cusp, J. Geophys. Res., 108, 1028, doi:10.1029/2002JA009476, 2003.

Haerendel, G., Paschmann, G., Sckopke, N., Rosenbauer, H., and Hedgecock, P.: The Frontside Boundary Layer of the Magnetosphere and the Problem of Reconnection, J. Geophys. Res., 83, 3195–3216, 1978.

Hansen, A. M., Bahnsen, A., and D'Angelo, N.: The Cusp-Magnetosheath Interface, J. Geophys. Res., 81, 556–561, 1976.

Lavraud, B., Dunlop, M. W., Phan, T. D., Rème, H., Bosqued, J.-M., Dandouras, I., Sauvaud, J.-A., Lundin, R., Taylor, M. G. G. T., Cargill, P. J., Mazelle, C., Escoubet, C. P., Carlson, C. W., McFadden, J. P., Parks, G. K., Moebius, E., Kistler, L. M., Bavassano-Cattaneo, M.-B., Korth, A., Klecker, B., and Balogh, A.: Cluster observations of the exterior cusp and its surrounding boundaries under northward IMF, Geophys. Res. Lett., 29, 56-1, 2002.

Lavraud, B., Fedorov, A., Budnik, E., Grigoriev, A., Cargill, P. J., Dunlop, M. W., Rème, H., Dandouras, I., and Balogh, A.: Cluster survey of the high-altitude cusp properties: a three-year statistical study, Ann. Geophys., 22, 3009–3019, doi:10.5194/angeo-22-3009-2004, 2004a.

Lavraud, B., Phan, T. D., Dunlop, M. W., Taylor, M. G. G. G. T., Cargill, P. J., Bosqued, J.-M., Dandouras, I., Rème, H., Sauvaud, J.-A., Escoubet, C. P., Balogh, A., and Fazakerley, A.: The exterior cusp and its boundary with the magnetosheath: Cluster multi-event analysis, Ann. Geophys., 22, 3039–3054, doi:10.5194/angeo-22-3039-2004, 2004b.

Lavraud, B., Fedorov, A., Budnik, E., Thomsen, M. F., Grigoriev, A., Cargill, P. J., Dunlop, M. W., Rème, H., Dandouras, I., and Balogh, A.: High altitude cusp flow dependence on IMF orientation: A 3 year Cluster statistical study, J. Geophys. Res., 110, A02209, doi:10.1029/2004JA010804, 2005.

Lockwood, M. and Smith, M.: The Variation of Reconnection Rate at the Dayside Magnetopause and Cusp Ion Precipitation, J. Geophys. Res., 97, 14841–14847, 1992.

Newell, P. T. and Meng, C.-I.: Cusp width and B(z) – Observations and a conceptual model, J. Geophys. Res., 92, 13673–13678, doi:10.1029/JA092iA12p13673, 1987.

Newell, P. T. and Meng, C. I.: Ionospheric Projections of Magnetospheric Regions under Low and High Solar Wind Pressure Conditions, J. Geophys. Res., 99, 273–286, 1994.

Newell, P., Meng, C.-I., Sibeck, D., and Lepping, R.: Some Low-Altitude Dependencies on the Interplanetary Magnetic Field, J. Geophys. Res., 94, 8921–8927, 1989.

Newell, P. T., Ruohoniemi, J. M., and Meng, C.-I.: Maps of precipitation by source region, binned by IMF, with inertial convection streamlines, J. Geophys. Res. (Space Physics), 109, A10206,

doi:10.1029/2004JA010499, 2004.

Niehof, J. T., Fritz, T. A., Friedel, R. H. W., and Chen, J.: Interdependence of magnetic field and plasma pressures in cusp diamagnetic cavities, J. Geophys. Res., 35, L11101, doi:10.1029/2008GL033589, 2008.

Niehof, J. T., Fritz, T. A., Friedel, R. H. W., and Chen, J.: Size and location of cusp diamagnetic cavities observed by Polar, J. Geophys. Res. (Space Physics), 115, A07201, doi:10.1029/2009JA014827, 2010.

Nykyri, K., Otto, A., Adamson, E., Dougal, E., and Mumme, J.: Cluster observations of a cusp diamagnetic cavity: Structure, size and dynamics, J. Geophys. Res., 116, A03228, doi:10.1029/2010JA015897, 2011a.

Nykyri, K., Otto, A., Adamson, E., and Tjulin, A.: On the origin of fluctuations in the cusp diamagnetic cavity, J. Geophys. Res. (Space Physics), 116, A06208, doi:10.1029/2010JA015888, 2011b.

Onsager, T. G., Kletzing, C. A., Austin, J. B., and Mackiernan, H.: Model of magnetosheath plasma in the magnetosphere – Cusp and mantle particles at low-altitudes, J. Geophys. Res., 20, 479–482, doi:10.1029/93GL00596, 1993.

Onsager, T., Scudder, J., Lockwood, M., and Russell, C.: Reconnection at the high latitude magnetopause during northward interplanetary magnetic field conditions, J. Geophys. Res., 106, A11, doi:10.1029/2000JA000444, 2001.

Paschmann, G., Haerendel, G., Sckopke, N., Rosenbauer, H., and Hedgecock, P.: Plasma and Magnetic Field Characteristics of the Distant Polar Cusp near Local Noon: The Entry Layer, J. Geophys. Res., 81, 2883–2899, 1976.

Peterson, W. K. and Trattner, K. J.: Sources of plasma in the high altitude cusp, J. Atmos. Solar-Terr. Physics, in press, doi:10.1016/j.jastp.2011.07.001, 2011.

Petschek, H. E.: Magnetic Field Annihilation, NASA Special Publication, 50, 425, 1964.

Pitout, F., Escoubet, C. P., Bogdanova, Y. V., Georgescu, E., Fazakerley, A. N., and Rème, H.: Response of the mid-altitude cusp to rapid rotations of the IMF, Geophys. Res. Lett., 33, 11107, 2006a.

Pitout, F., Escoubet, C. P., Klecker, B., and Rème, H.: Cluster survey of the mid-altitude cusp: 1. size, location, and dynamics, Ann. Geophys., 24, 3011–3026, doi:10.5194/angeo-24-3011-2006, 2006b.

Rosenbauer, H., Gruenwaldt, H., Montgomery, M. D., Paschmann, G., and Sckopke, N.: Heos 2 plasma observations in the distant polar magnetosphere - The plasma mantle, J. Geophys. Res., 80, 2723–2737, doi:10.1029/JA080i019p02723, 1975.

Russell, C. T.: Polar Eyes the Cusp, Cluster-II Workshop: Multiscale/Multipoint Plasma Measurements, Proceedings of the Workshop held at Imperial College, London, UK, 22–24 September 1999, 449, 47, 2000.

Sandholt, P. E., Farrugia, C. J., Burlaga, L. F., Holtet, J. A., Moen, J., Lybekk, B., Jacobsen, B., Opsvik, D., Egeland, A., and Lepping, R.: Cusp/cleft auroral activity in relation to solar wind dynamic pressure, interplanetary magnetic field B_z and B_y, J. Geophys. Res., 99, 17323–17342, 1994.

Savin, S. P., Romanov, S. A., Fedorov, A., Zelenyi, L., Klimov, S. I., Yermolaev, Y. I., Budnik, E. Y., Nikolaeva, N. S., Russell, C. T., Zhou, X.-W., Urquhart, A. L., and Reiff, P. H.: The Cusp/Magnetosheath Interface on May 29, 1996: Interball 1 and Polar Observations, Geophys. Res. Lett., 25, 2963–2966, 1998.

Scarf, F. L., Fredricks, R. W., Neugebauer, M., and Russell, C. T.: Plasma Waves in the Dayside Polar Cusp, 2. Magnetopause and Polar Magnetosheath, J. Geophys. Res., 79, 511–520, 1974.

Sonnerup, B. U. O. and Cahill, L. J.: Magnetopause Structure and Attitude from Explorer 12 Observations, J. Geophys. Res., 72, 171–183, 1967.

Trattner, K. J., Fuselier, S. A., and Petrinec, S. M.: Location of the reconnection line for northward interplanetary magnetic field, J. Geophys. Res., 109, A03219, doi:10.1029/2003JA009975, 2004.

Trattner, K. J., Petrinec, S. M., Peterson, W. K., Fuselier, S. A., and Reme, H.: Tracing the location of the reconnection site from the northern and southern cusps, J. Geophys. Res. (Space Physics), 111, A11211, doi:10.1029/2006JA011673, 2006.

Walters, G. K.: On the Existence of a second standing shock wave attached to the magnetosphere, J. Geophys. Res., 71, 1341–1344, 1966.

Woch, J. and Lundin, R.: Magnetosheath Plasma Precipitation in the Polar Cusp and its Control By the Interplanetary Magnetic Field, J. Geophys. Res., 97, 1421–1430, 1992.

Yamauchi, M. and Lundin, R.: Classification of Large-scale and Meso-scale Ion Dispersion Patterns Observed BY Viking over the Cusp-mantle Region, Kluwer Academic Publishers, 1994.

Yamauchi, M. and Lundin, R.: The Wave-Assisted Cusp Model: Comparison to Low-Altitude Observations, Phys. Chem. Earth, 22, 729–734, 1997.

Yamauchi, M., Nilsson, H., Eliasson, L., Norberg, O., Boehm, M., Clemmons, J. H., Lepping, R. P., Blomberg, L., Ohtani, S.-I., Yamamoto, T., Mukai, T., Terasawa, T., and Kokubun, S.: Dynamic response of the cusp morphology to the solar wind: A case study during passage of the solar wind plasma cloud on February 21, 1994, J. Geophys. Res., 101, 24675–24687, 1996.

Zhang, H., Dunlop, M. W., Zong, Q.-G., Fritz, T. A., Balogh, A., and Wang, Y.: Geometry of the High-latitude Magnetopause as Observed by Cluster, J. Geophys. Res., 112, 2204–2210, 2007.

Zhou, X. W. and Russell, C. T.: The location of the high-latitude polar cusp and the shape of the surrounding magnetopause, J. Geophys. Res., 102, 105–110, 1997.

Zhou, X. W., Russell, C. T., Le, G., Fuselier, S. A., and Scudder, J. D.: Solar wind control of the polar cusp at high altitude, J. Geophys. Res., 105, 245–251, 2000.